Nonequilibrium steady states of Bose-Einstein condensates with a local particle loss in double potential barriers

Masaya Kunimi and Ippei Danshita

Phys. Rev. A **100**, 063617 — Published 6 December 2019

DOI: 10.1103/PhysRevA.100.063617

Non-equilibrium steady states of Bose-Einstein condensates with a local particle loss in double potential barriers

Masaya Kunimi[1,*] and Ippei Danshita[2]

[1] *Yukawa Institute for Theoretical Physics, Kyoto University, Kyoto 606-8502, Japan*
[2] *Department of Physics, Kindai University, Higashi-Osaka, Osaka 577-8502, Japan*

(Dated: October 28, 2019)

We investigate stability of non-equilibrium steady states of Bose-Einstein condensates with a local one-body loss in the presence of double potential barriers. We construct an exactly solvable mean-field model, in which the local loss and the potential barriers take the form of δ-function. Using the exact solutions of our model, we show that there are parameter regions where two steady-state solutions are dynamically stable, i.e., the model exhibits bistability. We also find that unidirectional hysteresis phenomena appear when the local-loss rate is varied in some parameter region.

I. INTRODUCTION

Ultracold gases are well known as coherent quantum systems with high controllability [1]. Ultracold gases are confined in a vacuum chamber by using magnetic fields or laser beams such that they are well decoupled from environments. This means that the ultracold gases are regarded as isolated quantum systems [2]. Many interesting phenomena have been studied in the context of the isolated quantum systems, such as thermalization [2–6] and many-body localization [7–12].

Recent technological advances in ultracold atom experiments allow us to introduce couplings to environment, namely dissipation, in a well controlled manner [13–20]. This means that we can switch ultracold gases from the isolated systems to controllable open many-body quantum systems [21–24]. The dissipation can be regarded as continuous measurements. When the dissipation is strong compared to other energy scales of the systems, the quantum Zeno effects occur [25], which suppress coherent processes such as tunneling. These effects have been observed in ultracold-gas experiments [13–18, 20, 26]. It is also worth mentioning that the controllable dissipations provide us new possibilities for exploring novel quantum systems, such as $\mathcal{PT}$ symmetric systems [27–31] and non-hermitian quantum systems [32–34].

Recently, the experimental group at Technische Universitat Kaiserslauten has observed bistability in a Bose-Einstein condensate (BEC) with a local particle loss confined in a one-dimensional optical lattice [18]. The local particle loss can be realized by focusing an electron beam on the central site of the optical lattice. They prepared two-different initial conditions. One is that the central site of the optical lattice is occupied by the particles and the other is that the central site is almost empty. Measuring the particle number of the central site by using scanning electron microscopy techniques, they have observed two different stable states. In the small (strong) dissipation regime, the occupied (empty) state is realized regardless of the initial conditions. On the other hand, in the intermediate dissipation strength, the two-different stable states are realized depending on the initial states. This means that the system exhibits bistability.

This experiment can be understood as a problem of stability of supercurrents under particle losses. Because the local particle loss induces the density difference between the central site and the others, the supercurrent flows from the surrounding sites into the central sites. The results observed in the experiment indicate that particle losses produce nontrivial effects to superfluidity. In fact, our previous work also showed that global three-body losses induce supercurrent decay in a ring trap [35].

In previous theoretical studies [36, 37], it has been shown that in the absence of optical lattice potentials, which are described by a real-number external field in the Gross-Pitaevskii (GP) equation, the system does not exhibits a discontinuous jump of the density under a local one-body loss associated with the bistability when the strength of the dissipation is varied. This is contrary to the experiment [18], in which an optical lattice potential is present. In this work, we construct a simple model that is analytically solvable and exhibits the discontinuous jump associated with the bistability. Specifically, we use a one-dimensional GP equation with a local one-body loss and double potential barriers, which are respectively described by pure imaginary and real delta function potentials. On the basis of semi-analytical solutions of our model, we indeed show that the inclusion of the double potential barriers lead to the emergence of bistability accompanied by the discontinuous jump. In addition, we find unidirectional hysteresis phenomena in our systems. These phenomena are called anomalous hysteresis [38–40].

This paper is organized as follows. In Sec. II, we explain the problem that we consider and its formulation based on a dissipative GP equation, which describes BEC with a local particle loss. In Sec. III A, using the exact solution of the GP equation, we briefly review impor-

*Electronic address: E-mail:kunimi@ims.ac.jp; Present address : Department of Photo-Molecular Science, Institute for Molecular Science, National Institutes of Natural Sciences, Myodaiji, Okazaki 444-8585, Japan

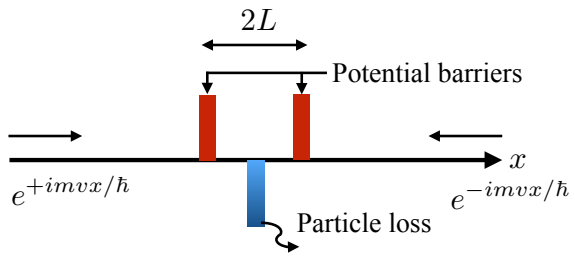

FIG. 1: (Color online) Schematic picture for our setup.

tant properties of the BEC in the absence of the double potential barriers. In Sec. III B, we obtain exact solutions of the GP equation in the presence of the double potential barriers in order to discuss the stability of non-equilibrium steady states of the BEC. In Sec. III C, we show that our system exhibits the anomalous hysteresis phenomena. In Sec. IV, we summarize our results. In the appendix, we explain how to perform the stability analysis of stationary solutions of the GP equation and the details of the derivations of the exact solution of the GP equation.

II. MODEL

In this paper, we consider a one-dimensional GP equation with a local one-body loss term and double-potential-barrier terms:

$$i\hbar\frac{\partial}{\partial t}\psi(x,t) = \left[-\frac{\hbar^2}{2M}\frac{\partial^2}{\partial x^2} + U(x) + g|\psi(x,t)|^2\right]\psi(x,t), \tag{1}$$

$$U(x) \equiv -\frac{i\hbar\gamma_0}{2}\delta(x) + U_0[\delta(x-L)+\delta(x+L)], \tag{2}$$

where M is the mass of the atom, $g>0$ is the two-body interaction coefficient, and $\psi(x,t)$ is the order parameter of the BEC. The dissipation term takes the form of the delta function localized at $x=0$ and $\gamma_0 \geq 0$ is the strength of the dissipation. The two potential barriers located at $x=\pm L$ are added for mimicking the density dips near the local loss created by the optical lattice in the experiment [18]. Their strength is denoted by $U_0 \geq 0$. This dissipative GP equation can be derived by the mean-field approximation of the Lindblad equation with the local one-body loss term (see details for supplemental material of Ref. [14]).

In the main part of this paper, we consider stability of non-equilibrium steady states of BEC, in which a stationary supercurrent flows into the location of the particle loss. Such states are represented as solutions of the time-independent GP equation, which is derived by inserting $\psi(x,t) = \Psi(x)e^{-i\mu t/\hbar}$ into Eq. (1):

$$\left[-\frac{\hbar^2}{2M}\frac{d^2}{dx^2} + U(x) - \mu + g|\Psi(x)|^2\right]\Psi(x) = 0, \tag{3}$$

where μ is the chemical potential.

We set the boundary condition at $x \to \pm\infty$ as (see also Fig. 1)

$$\Psi(x) \xrightarrow{x\to\pm\infty} \sqrt{n_\infty}e^{-iMv_\infty|x|/\hbar}e^{i\varphi_\pm}, \tag{4}$$

where $n_\infty \geq 0$ is the mean particle density at infinity, $v_\infty \geq 0$ is the magnitude of the flow velocity at infinity, and $\varphi_\pm$ is the phase. From this boundary condition, we obtain the chemical potential:

$$\mu = gn_\infty + \frac{1}{2}Mv_\infty^2. \tag{5}$$

The velocity v_∞ is determined by the boundary conditions due to the delta functions, which are given by

$$\Psi(\pm L+0) = \Psi(\pm L-0), \quad \Psi(+0) = \Psi(-0), \tag{6}$$

$$\frac{\hbar^2}{2M}\left[\left.\frac{d\Psi(x)}{dx}\right|_{x=\pm L+0} - \left.\frac{d\Psi(x)}{dx}\right|_{x=\pm L-0}\right] = U_0\Psi(\pm L), \tag{7}$$

$$\frac{\hbar^2}{2M}\left[\left.\frac{d\Psi(x)}{dx}\right|_{x=+0} - \left.\frac{d\Psi(x)}{dx}\right|_{x=-0}\right] = -\frac{i\hbar\gamma_0}{2}\Psi(0). \tag{8}$$

We check the stability of the obtained stationary solutions by the numerical simulations of the time-dependent GP equation. See the details for Appendix A.

In the end of this section, we remark on a crucial difference between our model and the actual experimental setup. In our setup, the particles are lost at the origin and provided at the infinity [see Eq. (4)]. This fact can be easily seen by writing down the equation of continuity:

$$\frac{\partial}{\partial t}n(x,t) = -\frac{\partial}{\partial x}J(x,t) - \gamma_0\delta(x)n(x,t), \tag{9}$$

$$n(x,t) \equiv |\psi(x,t)|^2, \tag{10}$$

$$J(x,t) \equiv -\frac{i\hbar}{2M}\left[\psi^*(x,t)\frac{\partial}{\partial x}\psi(x,t) - \text{c.c.}\right], \tag{11}$$

where $n(x,t)$ and $J(x,t)$ are the particle density and the current density, respectively. Integrating Eq. (9) over $(-\infty,+\infty)$ yields

$$\frac{d}{dt}N(t) = -[J(+\infty,t) - J(-\infty,t)] - \gamma_0 n(0,t), \tag{12}$$

where $N(t) \equiv \int_{-\infty}^{+\infty} dx[n(x,t)-n_\infty]$ is the total particle number difference at time t [41]. The first and second terms in the right hand side of Eq. (12) represent the gain of the particles from the boundaries and the third one represents the loss of the particles at $x=0$. This equation shows that non-equilibrium steady states can be realized when the loss and gain of the particles are balanced.

In the experiment, the BEC confined in the trap potential with the local particle loss. Because there is no particle source in contrast to our theoretical setup, the total particle number in the trap monotonically decreases.

Hence, strictly speaking, the stationary states cannot exist except a vacuum state (no particle in the trap). However, according to the inset of Fig. 2 (a) in Ref. [18], we can see that the particle number at the central site is almost stationary in the time scale $40 \sim 60$ ms. In this time scale, the particle loss and the hopping from the adjacent sites to the central site are balanced. As long as we focus on the vicinity of the central site, the systems can be approximated as non-equilibrium steady states. Stationary states in our model correspond to these non-equilibrium steady states.

Another difference is the width of the local dissipation term. As described above, we assume that the local dissipation is given by the delta function. This treatment can be justified when the width of the dissipation is much smaller than the healing length. However, in the experiment, the width of the dissipation is about $O(0.1\mu\mathrm{m})$ [14]. Because the healing length of the experiment is $O(0.1\mu\mathrm{m})$, the dissipation in the experiment cannot be regarded as the delta function. We will also remark the effects of the finite width in Sec. III B.

III. RESULTS

A. In the absence of the double potential barriers

We first review exact solutions in the absence of the double potential barriers, which have been derived in some previous works [36, 37], for reader's convenience before showing our results.

There are three kind of exact solutions in the absence of the potential barriers ($U_0 = 0$). One is a plane wave (PW) solution:

$$\Psi_{\mathrm{PW}}(x) = \sqrt{n_\infty} e^{-iMv_\infty |x|/\hbar}, \tag{13}$$

$$v_\infty = \frac{\gamma_0}{2}. \tag{14}$$

The second one is a dark soliton (DS) solution:

$$\Psi_{\mathrm{DS}}(x) = \sqrt{n_\infty}\tanh(x/\xi), \tag{15}$$

$$v_\infty = 0, \tag{16}$$

where $\xi \equiv \hbar/\sqrt{Mgn_\infty}$ is the healing length. The last one is a gray soliton (GS) solution:

$$\Psi_{\mathrm{GS}}(x) = \sqrt{n_\infty} e^{-iMv_\infty |x|/\hbar}\left[i\frac{v_\infty}{v_\mathrm{s}} + f(x)\right], \tag{17}$$

$$f(x) \equiv \sqrt{1-\left(\frac{v_\infty}{v_\mathrm{s}}\right)^2}\tanh\left[\sqrt{1-\left(\frac{v_\infty}{v_\mathrm{s}}\right)^2}\frac{|x|}{\xi}\right], \tag{18}$$

$$v_\infty = \frac{2v_\mathrm{s}^2}{\gamma_0}, \tag{19}$$

where $v_\mathrm{s} \equiv \sqrt{gn_\infty/M}$ is the sound velocity. We can easily check that these expressions satisfy the GP Eq. (3).

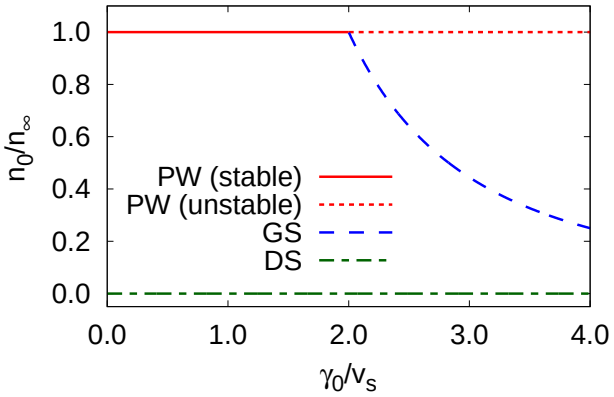

FIG. 2: (Color online) Density at the origin as a function of the dissipation strength. The red solid (dotted), blue dashed, and green dashed-dotted lines represent the (un)stable PW solutions, the GS solutions, and the DS solutions, respectively.

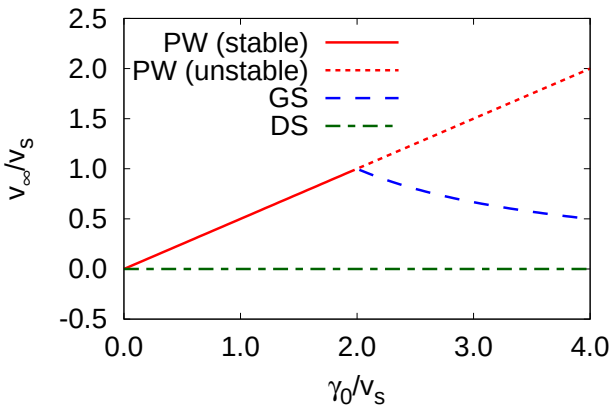

FIG. 3: (Color online) Magnitude of the flow velocity at infinity as a function of the dissipation strength. The red solid (dotted), blue dashed, and green dashed-dotted lines represent the (un)stable PW solutions, the GS solutions, and the DS solutions, respectively.

We note that the PW and DS solutions exist for arbitrarily parameters and the GS solution exists for $\gamma_0 > 2v_\mathrm{s}$.

Here, we define the density at the origin as $n_0 \equiv |\Psi(x=0)|^2$, which corresponds to the density at the central site in the experiment [18]. We plot n_0 as a function of γ_0 in Fig. 2, which we call a n_0-γ_0 diagram. This result shows that the system exhibits the bistability for the whole γ_0 region. For $\gamma_0 \le 2v_\mathrm{s}$, the PW and the DS states are stable and for $\gamma_0 > 2v_\mathrm{s}$, the GS and the DS states are stable. We can see the unstable PW states for $\gamma_0 > 2v_\mathrm{s}$. This can be understood by the velocity shown in Fig. 3. The velocity of the PW state is given by Eq. (14) which is proportional to the dissipation strength γ_0. When the velocity exceeds the sound velocity, which is the Landau critical velocity of uniform superfluids [42, 43], the PW state becomes energetically unstable.

The GS state emerges at $\gamma_0 = 2v_\mathrm{s}$ ($v_\infty = v_\mathrm{s}$). The velocity of the GS state is a monotonically decrease function of γ_0 [see Eq. (19)]. We can interpret this behavior

as follows. Suppose that we start with the PW state at $\gamma_0 = 0$. When we increase the dissipation strength from $\gamma_0 = 0$, the superflow velocity becomes large and then reaches the Landau critical velocity. Finally, the PW states become unstable and bifurcate into the unstable PW branch and the stable GS branch.

In the DS states, the density at the origin is always zero. This means that the DS states do not feel the dissipation. In fact, the boundary condition (8) is satisfied in the DS solution (15) for whole γ_0. Therefore, the DS states always exist regardless of the dissipation strength.

B. In the presence of the double potential barriers

Here, we show the results in the presence of the double potential barriers. We assume that a functional form of the stationary solution is given by an even function or an odd function. Owing to this assumption, it is sufficient to consider only the $x \geq 0$ region. Because the potentials are only the delta function type, we can separately solve the GP equation in an inside region ($0 \leq x \leq L$) and an outside region ($x > L$). After obtaining the solutions of each region, we connect them by using the boundary conditions (6), (7), and (8). Such techniques to solve the GP equation with delta function potentials have been developed in the context of the Josephson junction systems [44–62]. For convenience, we introduce the following variables

$$\Psi(x) \equiv \begin{cases} \Psi_{\rm in}(x) \equiv \sqrt{n_{\rm in}(x)} e^{i\varphi_{\rm in}(x)}, & \text{for } 0 \leq x \leq L \\ \Psi_{\rm out}(x) \equiv \sqrt{n_{\rm out}(x)} e^{i\varphi_{\rm out}(x)}, & \text{for } x > L \end{cases}. \tag{20}$$

First, we consider the even function case. The solution of the outside region is given by

$$\frac{n_{\rm out}(x)}{n_\infty} = \left(\frac{v_\infty}{v_{\rm s}}\right)^2 + \left[1 - \left(\frac{v_\infty}{v_{\rm s}}\right)^2\right] \times \tanh^2\left[\sqrt{1 - \left(\frac{v_\infty}{v_{\rm s}}\right)^2}\frac{x - L + x_+}{\xi}\right], \tag{21}$$

$$\varphi_{\rm out}(x) = \varphi_L - \frac{M v_\infty (x - L)}{\hbar} - \tan^{-1}\left[\frac{G(x + x_+)}{v_\infty / v_{\rm s}}\right] + \tan^{-1}\left[\frac{G(L + x_+)}{v_\infty / v_{\rm s}}\right], \tag{22}$$

$$\frac{x_+}{\xi} \equiv \frac{1}{\sqrt{1 - \left(\frac{v_\infty}{v_{\rm s}}\right)^2}} \times \tanh^{-1}\left[\sqrt{\frac{n_L/n_\infty - (v_\infty/v_{\rm s})^2}{1 - (v_\infty/v_{\rm s})^2}}\right], \tag{23}$$

$$G(x) \equiv \sqrt{1 - \left(\frac{v_\infty}{v_{\rm s}}\right)^2} \tanh\left[\sqrt{1 - \left(\frac{v_\infty}{v_{\rm s}}\right)^2}\frac{x - L}{\xi}\right], \tag{24}$$

where $\varphi_L \equiv \varphi(x = L)$, $n_L \equiv n(x = L)$ will be determined by using the boundary conditions below. v_∞ is given by

$$v_\infty = \frac{1}{2}\frac{n_0}{n_\infty}\gamma_0. \tag{25}$$

This relation can be derived by using the assumption of the even function, the expression of the current density, and the boundary conditions (8). The details of the derivation of the outside solution and Eq. (25) are summarized in Appendix B.

In the inside region, we find four types of the inside solutions. However, only two solutions appear in the parameter regions of our interest, where $0 \leq \gamma_0/v_{\rm s} \leq 4$ and $0 \leq n_0/n_\infty \leq 1$. Then we consider two types of the

solutions:

$$\frac{n_{\rm in}^{(1)}(x)}{n_\infty} = A - \left(A - \frac{n_0}{n_\infty}\right) {\rm nd}^2(\Delta^{1/4}x/\xi|m_1), \tag{26}$$

$$\varphi_{\rm in}^{(1)}(x) = -\frac{1}{2A}\frac{n_0}{n_\infty}\frac{\gamma_0}{v_{\rm s}}\frac{x}{\xi} - \frac{1}{2\Delta^{1/4}}\frac{\gamma_0}{v_{\rm s}}\frac{A - n_0/n_\infty}{A} \times \Pi[m_1 A/(n_0/n_\infty); {\rm am}(\Delta^{1/4}x/\xi|m_1)|m_1], \tag{27}$$

$$m_1 \equiv 1 - \frac{A - n_0/n_\infty}{\sqrt{\Delta}}, \tag{28}$$

$$\frac{n_{\rm in}^{(2)}(x)}{n_\infty} = \frac{n_0}{n_\infty} + \left(B - \frac{n_0}{n_\infty}\right) {\rm sn}^2(\Delta^{1/4}x/\xi|m_2), \tag{29}$$

$$\varphi_{\rm in}^{(2)}(x) = -\frac{1}{2\Delta^{1/4}}\frac{\gamma_0}{v_{\rm s}} \times \Pi\left[\frac{B - n_0/n_\infty}{n_0/n_\infty}; {\rm am}(\Delta^{1/4}x/\xi|m_2)\middle| m_2\right], \tag{30}$$

$$m_2 \equiv \frac{B - n_0/n_\infty}{A - n_0/n_\infty}, \tag{31}$$

where we set the origin of the phase as $\varphi_{\rm in}^{(i)}(x=0) = 0$ and used the Jacobi elliptic functions ${\rm sn}(x|m)$ and ${\rm nd}(x|m) \equiv 1/{\rm dn}(x|m)$, the incomplete elliptic integral of the third kind $\Pi(n;\phi|m)$, and Jacobi amplitude function ${\rm am}(x|m)$. The notations of the Jacobi elliptic functions and the elliptic integrals are followed by Abramowitz and Stegun [63]. We also used the following quantities:

$$A \equiv \frac{1}{2}\left[2 + \frac{1}{4}\left(\frac{\gamma_0}{v_{\rm s}}\right)^2\left(\frac{n_0}{n_\infty}\right)^2 - \frac{n_0}{n_\infty} + \sqrt{\Delta}\right], \tag{32}$$

$$B \equiv \frac{1}{2}\left[2 + \frac{1}{4}\left(\frac{\gamma_0}{v_{\rm s}}\right)^2\left(\frac{n_0}{n_\infty}\right)^2 - \frac{n_0}{n_\infty} - \sqrt{\Delta}\right], \tag{33}$$

$$\Delta \equiv \left[\frac{n_0}{n_\infty} - 2 - \frac{1}{4}\left(\frac{\gamma_0}{v_{\rm s}}\right)^2\left(\frac{n_0}{n_\infty}\right)^2\right]^2 - \left(\frac{\gamma_0}{v_{\rm s}}\right)^2\frac{n_0}{n_\infty}. \tag{34}$$

From the above results and the boundary condition (6), n_L and φ_L are determined by

$$n_L = n_{\rm in}^{(i)}(x=L), \quad \varphi_L = \varphi_{\rm in}^{(i)}(x=L). \tag{35}$$

Next, we consider the odd function case. From this assumption, we obtain $\Psi(x=0) = 0$. This means that the odd function solution does not depend on γ_0 (see the descriptions of the DS in Sec. III A). From the equation of continuity, the current density is independent of x. In this case, $J(x) = 0$ because $\Psi(0) = 0$. Therefore, the odd function solution does not carry a supercurrent and we can take $\Psi(x)$ as a real function without loss of generality. The solution is given by

$$\Psi_{\rm out}(x) = \sqrt{n_\infty}\tanh\left(\frac{x - L + x_0}{\xi}\right)e^{i\varphi_0}, \tag{36}$$

$$\Psi_{\rm in}(x) = \sqrt{n_\infty}\sqrt{\frac{2m_0}{1+m_0}}{\rm sn}\left(\sqrt{\frac{2}{1+m_0}}\frac{x}{\xi}\middle| m_0\right), \tag{37}$$

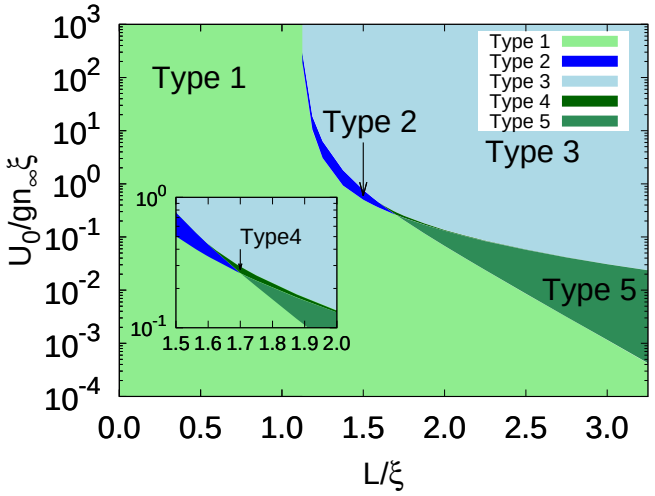

FIG. 4: (Color online) State phase diagram for U_0 vs L. The inset shows the magnified view abound the type 4 region.

where $\varphi_0 = 0$ or π and x_0 and m_0 are constants. φ_0 and x_0 are determined by the boundary condition (6):

$$\tanh\left(\frac{x_0}{\xi}\right)e^{i\varphi_0} = \sqrt{\frac{2m_0}{1+m_0}}{\rm sn}\left(\sqrt{\frac{2}{1+m_0}}\frac{L}{\xi}\middle| m_0\right). \tag{38}$$

Although the functional forms of the exact solution have been derived, n_0 (for the even function case) and m_0 (for the odd function case) have not been determined yet. These variables can be determined by solving the boundary condition (7). Unfortunately, we cannot solve Eq. (7) analytically. We numerically solve Eq. (7). The details of the derivations of these solutions are shown in Appendixes B and C.

Here, we remark the range of L. From Eqs. (26) and (29), we can find that the inside solutions have a periodicity $2K(m_1)\xi/\Delta^{1/4}$ and $2K(m_2)\xi/\Delta^{1/4}$ due to the properties of the Jacobi elliptic functions, where $K(\cdot)$ is the complete elliptic integral of the first kind. If L is much larger than these periods, we can expect that there are solutions that oscillate multiple times in the inside region. To avoid the complexity of the problem, we restrict the range of L as $0 \le L \lesssim 3.3$, which means that the number of oscillations in the inside region is less than one.

In the presence of the double potential barriers, we find five types of n_0-γ_0 diagrams. The parameter region for the n_0-γ_0 diagrams is shown in Fig. 4.

A typical diagram of the type 1 is shown in Fig. 5. In the type 1, we have two stable branches. One is the even function (upper one) and the other one is the odd function (lower one). The type 1 solution tends to exist in a region where U_0 is small. This means the type 1 can be interpreted as perturbed states of the $U_0 = 0$ states. In fact, the n_0-γ_0 diagram of Fig. 4 is similar to that of Fig 2 except the existence of the unstable PW branch.

The type 2 emerges in the adjacent region of the type

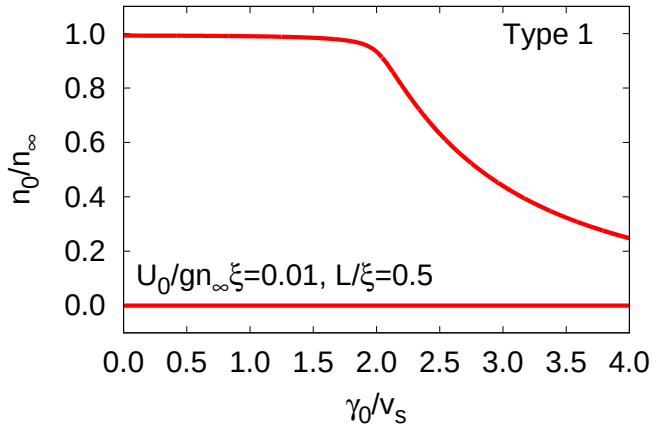

FIG. 5: (Color online) n_0-γ_0 diagram for $U_0 = 0.01gn_\infty\xi$ and $L = 0.5\xi$.

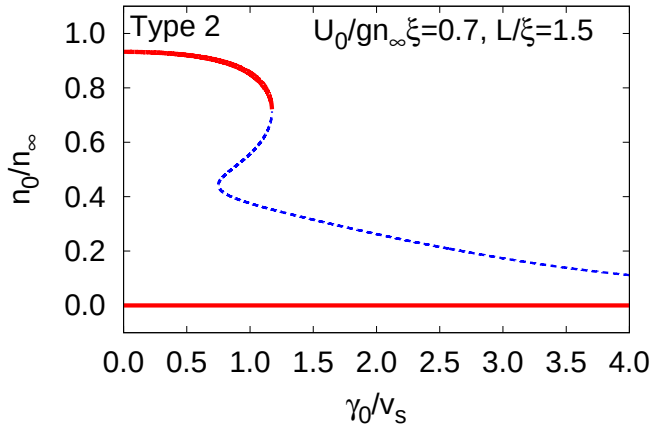

FIG. 6: (Color online) n_0-γ_0 diagram for $U_0 = 0.7gn_\infty\xi$ and $L = 1.5\xi$. The red solid and blue doted lines represent the stable and unstable states, respectively.

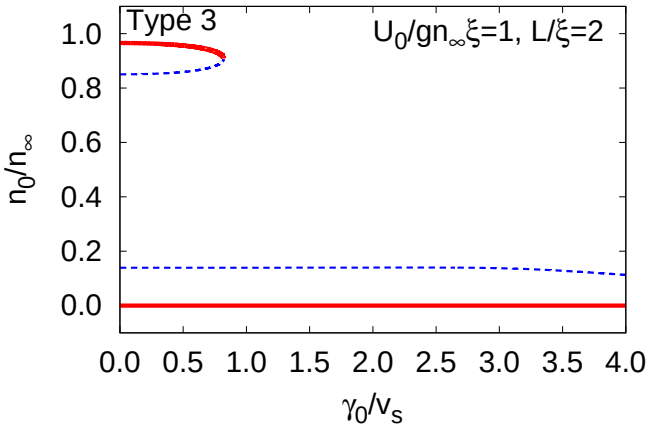

FIG. 7: (Color online) n_0-γ_0 diagram for $U_0 = 1gn_\infty\xi$ and $L = 2\xi$. The red solid and blue doted lines represent the stable and unstable states, respectively.

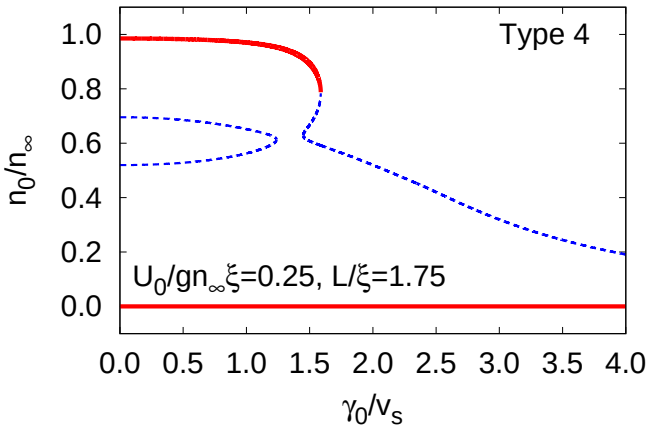

FIG. 8: (Color online) n_0-γ_0 diagram for $U_0 = 0.25gn_\infty\xi$ and $L = 1.75\xi$. The red solid and blue doted lines represent the stable and unstable states, respectively.

1. A typical n_0-γ_0 diagram is shown in Fig. 6. In the type 2, we can see the discontinuous jump between the upper branch and the lower branch. The similar discontinuous jump has been observed in the experiment [18]. In contrast, there is no discontinuous jump in the absence of the potential barriers (see Fig. 2). This result means that the discontinuous jump is due to the effects of the potential barriers.

We show a typical n_0-γ_0 diagram of type 3 in Fig. 7. In the type 3, the upper and lower branches are completely separated. We can see a saddle-node bifurcation in the upper branch, in which two fixed points collide with each other and annihilate [64]. This behavior is similar to that of the Josephson junction systems. Theoretically, these systems have been studied by using the GP equation or the Ginzburg-Landau equation with a single potential barrier [44–62]. In fact, our system can be regarded as a connection of two reverse Josephson junction systems via the local loss. The upper branch is reflected by the properties of the Josephson junction, i.e. superfluidity.

The type 4 emerges in a narrow region surrounded by the type 2, 3, and 5 (see the inset of Fig. 4). A typical n_0-γ_0 diagram is shown in Fig. 8. In the type 4, the upper and lower branches are similar to those of type 2 and one additional branch emerges between the upper and lower branches.

A typical n_0-γ_0 diagram of type 5 is shown in Fig. 9. The type 5 is located between the type 1 and type 4. The type 5 is similar to the type 4 except the upper branch. The upper branch of the type 5 is similar to that of the type 1.

From the above results, we can see the bistability for whole γ_0 in the type 1 and 5 and partial region in the type 2, 3, and 4. The difference between the presence and the absence of the potential barriers is the existence of the discontinuous jump, which can be seen in the type 2, 3, and 4.

Comparing our results with the experimental ones, we find that our results are in part inconsistent with the experiment [18]. In the small γ_0 region, while only one stable state was observed in the experiment, there are

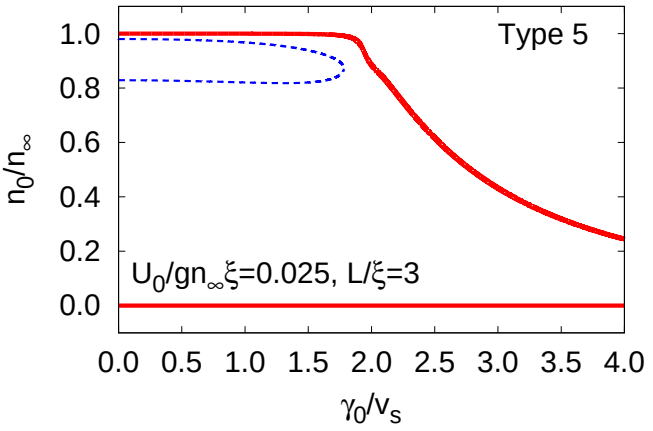

FIG. 9: (Color online) n_0-γ_0 diagram for $U_0 = 0.025gn_\infty\xi$ and $L = 3\xi$. The red solid and blue doted lines represent the stable and unstable states, respectively.

two stable states in our model, one of which is the DS state. One possible reason for this discrepancy is that the local particle loss is modeled as a delta-function form.

C. Anomalous hysteresis

In addition to the bistability, the present system exhibits a non-trivial hysteresis phenomenon, which is called anomalous hysteresis [38–40]. A feature of the anomalous hysteresis is unidirectionality. In the conventional hysteresis phenomena, if we observe a discontinuous jump from an initial phase to another phase by changing parameters sufficiently slowly, another jump going back to the initial phase exists along the reverse path in the parameter space. However, in the anomalous hysteresis, the discontinuous jump exists only in one direction. This phenomenon has been predicted in quantum phase transitions of dipolar or multi-component Bose gases in an optical lattice [38, 40] and frustrated magnets [39], and it can be understood within the framework of the Ginzburg-Landau theory.

Here, we focus on the type 3. The processes of the anomalous hysteresis are shown in Fig. 10. First, we prepare the initial state at point (1) shown in Fig. 10 (a). Then we increase γ_0 sufficiently slowly. When the dissipation strength reaches the critical value, the discontinuous jump occurs from the upper branch to the lower branch. After the discontinuous jump, we decrease the dissipation strength and finally reach the point (2) shown in Fig. 10 (a). Next, let us consider the inverse process, that is, the initial state is the point (2) in Fig. 10 (b) and the goal is the point (1) in Fig. 10 (b). However, this process is impossible because the lowest branch is stable for whole γ_0. This means that we cannot reach the point (1) starting from the point (2) as long as we consider sufficiently slow changes of the parameters. This is nothing but the anomalous hysteresis phenomenon as we mentioned above.

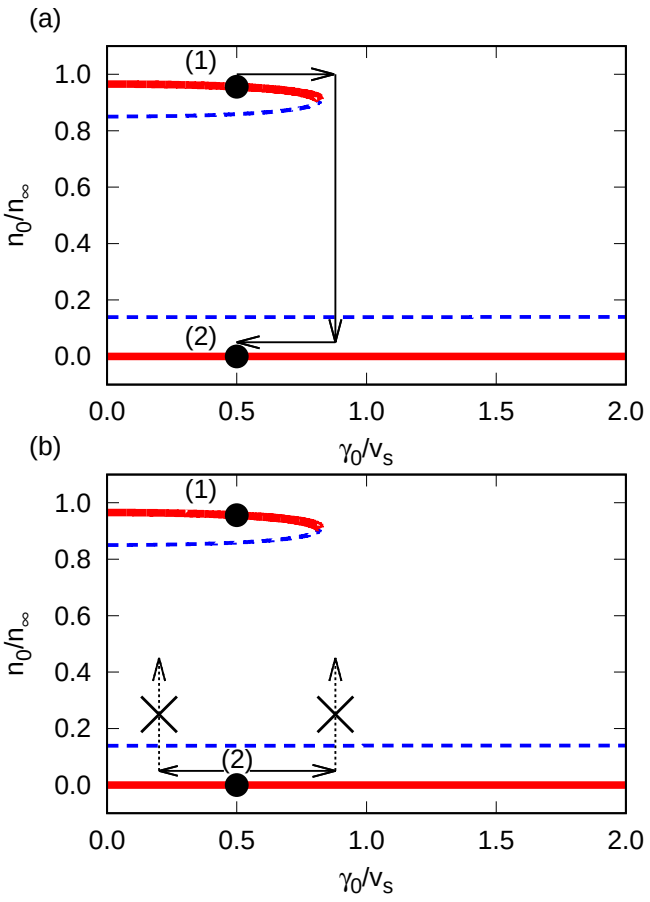

FIG. 10: (Color online) Anomalous hysteresis process. The parameters are the same as those of Fig. 7.

Here, we discuss the timescale of changing parameters. For example, let us consider the case shown in Fig. 10. The energy difference between the upper stable branch and the lower stable branch is given by the energy of the dark soliton, which is order of the chemical potential. In the actual experiments, the chemical potential is typically order of 1 kHz. The inverse of this energy scale gives us the timescale of changing parameters. Therefore, we should change the parameters within the timescale slower than 1ms. This condition can be easily satisfied in the cold gases experiments. We also remark the adiabatic condition of the system. The adiabatic condition of the present system, which corresponds to the condition where no excitation is present, is given by the Bogoliubov excitation. We can roughly estimate the timescale to be 100 ms for the system size $O(10\xi)$. This means that the Bogoliubov excitations are present in the experiment [18] because the experimental timescale is shorter than 100ms. Nevertheless, the hysteresis loop can be clearly observed. This indicates that the adiabaticity is not a necessary condition but sufficient condition for observing the hysteresis loop.

In the end of this section, we discuss feasibility for observing the anomalous hysteresis in experiment. Thus

far, the anomalous hysteresis has not been observed experimentally for the following reasons. For the case of the dipolar or multi-component Bose gases in the optical lattice [38, 40], the temperature in the optical lattice has not been lowered enough to observe the anomalous hysteresis. For the case of the frustrated magnets [39], it is difficult to tune the parameters to the optimal values for observing the anomalous hysteresis.

In contrast to the previous works, there is no difficulty in our model for achieving sufficiently low temperatures and optimal values of the parameters. However, the anomalous hysteresis has not been observed in the experiment [18]. There are a few possible reasons for this discrepancy. One is the effects of the harmonic trap. The presence of the trap potential may affect the hysteresis because it changes the boundary condition of the system. In our systems, we fix the wave function as the plane wave at the infinity. This means the particles are provided from the bath. This situation is different from the experimental setup, which is the isolated from the environment except the local loss. We also remark that this boundary condition produces an additional nonlinearity. The combination of the boundary conditions at infinity and at the origin determines the velocity at infinity [see Eq. (25)]. The velocity depends on the density at the origin. This constraint does not exist in the experimental setup. This difference may affect the existence of the anomalous hysteresis. Another one is the effects of optical lattices. The optical lattice extends all over the system. In contrast to this, in our system, the double delta potentials are localized near the center of the system. This difference may affect the hysteresis. In addition to these points, the width of the local dissipation may affects the stability as discussed in Sec. III B.

IV. SUMMARY AND FUTURE PROSPECT

We investigated stability of BEC with a local one-body loss in double potential barriers by using the mean-field approximation. We obtained the exact solutions of the GP equation in the presence of the delta function potentials with the pure imaginary and real coefficients, which are written by the Jacobi elliptic functions. We showed that there is a wide parameter region, in which two non-equilibrium steady states are dynamically stable, i.e., our model exhibits the bistability. We also found the anomalous hysteresis phenomena in our system.

As a future plan, we investigate the effects of the width of the local dissipation and the optical lattice potentials. These effects may change the stability of the present system. By studying these effects, we may clarify the origin of the bistability observed in the experiment.

It is interesting to extend our analysis to strongly correlated regimes. Our model is based on the mean-field theory, which can be justified only in the weakly-correlated regimes. Strongly-correlated non-equilibrium states are one of the most difficult problems in various fields. As a related topic to the bistability, negative differential conductivity is theoretically studied by using anti-de Sitter space/conformal field theory correspondence [65].

Another extension is to consider the effects of local multi-body losses, for example, two-body losses and three-body loses. Particularly, the controllable global two-body losses have been realized by using the photo-association laser [20]. By developing this kind of experimental techniques, controllable local two-body losses will be experimentally realized.

Acknowledgments

M. K. thanks D. A. Takahashi for his lecture of the Jacobi elliptic function, S. Takada for useful discussion, and T. Tomita for useful comments. M. K. was supported by Grant-in-Aid for JSPS Research Fellow Grant No. JP16J07240. I. D. was supported by KAKENHI grants from JSPS: Grants No. 15H05855, No. 25220711, No. 18K03492, and No. 18H05228, by research grant from CREST, JST, and by Q-LEAP program of MEXT, Japan.

Appendix A: Stability analysis

Here, we explain how to perform the stability analysis of the stationary state. To do this, we investigate real-time dynamics. However, we do not use Eq. (1) because of some technical reasons as described below.

The original problem is defined by an infinite size system. However, this system is not tractable numerically. Instead of considering the infinite systems, we consider the finite size system $(-L_{\rm s}, +L_{\rm s})$, where we take $L_{\rm s}$ about 100ξ. The equation considered here is given by

$$i\hbar\frac{\partial}{\partial t}\psi(x,t) = [1 - i\Gamma(x)]\mathcal{L}(x,t)\psi(x,t), \tag{A1}$$

$$\mathcal{L}(x,t) \equiv -\frac{\hbar^2}{2M}\frac{\partial^2}{\partial x^2} + U(x) - \mu(t) + g|\psi(x,t)|^2, \tag{A2}$$

$$\mu(t) \equiv gn_\infty + \frac{1}{2}Mv(t)^2, \tag{A3}$$

$$v(t) \equiv \frac{1}{2}\frac{n(0,t)}{n_\infty}\gamma_0, \tag{A4}$$

$$\Gamma(x) \equiv 2 + \tanh\left(\frac{x - L_{\rm d}}{W}\right) - \tanh\left(\frac{x + L_{\rm d}}{W}\right), \tag{A5}$$

where we introduce spatially varying dissipation term $\Gamma(x)$. The reason why we introduce the dissipation term is to avoid effects of the reflection of the boundary, which does not exist in the original problem. The functional form of the dissipation $\Gamma(x)$ is same as that used in Ref. [66]. The parameters are set to $L_{\rm d} = L_{\rm s}/2$ and

$W = 10\xi$. We note that the choice of these parameters are insensitive to the results as long as $L_{\rm d}, W \gg \xi$ are satisfied. We also introduce the time dependence of the chemical potential to converge the stationary solution at the long time. The boundary condition at the edge of the system is given by

$$\left.\frac{\partial\psi(x,t)}{\partial x}\right|_{x=\pm L_{\rm s}} = \mp i\frac{Mv(t)}{\hbar}\psi(\pm L_{\rm s},t). \tag{A6}$$

We numerically solve Eq. (A1) by using the fourth-order Runge-Kutta method. The centered difference method is used for the space discretization. We use the number of meshes for $N_x = 2001 \sim 64001$. In this calculation, we approximate the delta function as the Kronecker $\delta(x - x_j) \simeq (1/\Delta x)\delta_{i,j}$, where $x_i \equiv \Delta x \times i$ [$i = -(N_x - 1)/2, \cdots, +(N_x - 1)/2$] and Δx is the mesh size. We write the discretized wave function at the mesh i and time t as $\psi_i(t)$. We have checked that the analytically obtained stationary solutions and the numerically obtained stationary solutions are good agreement.

The procedure of the stability analysis is as follows. We use the initial conditions as the exact solution plus small random noise. That is, the initial condition is given by $\psi_j(0) = \psi_{\rm exact}(x_j) + \epsilon_j^{\rm R} + i\epsilon_j^{\rm I}$, where $\psi_{\rm exact}(x_j)$ is the exact solution at the mesh j and $\epsilon_j^{\rm R}$ and $\epsilon_j^{\rm I}$ are real values. We set $-10^{-4} \le \epsilon_j^{\rm R}, \epsilon_j^{\rm I} \le 10^{-4}$. Then we numerically calculate the real-time dynamics. After the long-time evolution [typically $1000\tau \sim 10000\tau$, where $\tau \equiv \hbar/(gn_\infty)$], we compare the final state with the initial state.

A typical example of the time evolution is shown in Fig. 11 (a). We see the dynamics of $n_0(t)$ for the type 3. We can see that the lowest branch (1) and uppermost branch (4) shown in red lines are stable against the small perturbation in the initial states. On the other hand, the branches (2) and (3) shown in blue lines are unstable. The instability sets in $t \sim 6000\tau$ for the branch (2) and $t \sim 20\tau$ for the branch (3), respectively. In order to quantify the instability, we calculate the following quantity [67]:

$$\lambda(t) \equiv \frac{\sum_i |\psi_i(t) - \psi_{\rm exact}(x_i)|^2}{\sum_i |\psi_i(0) - \psi_{\rm exact}(x_i)|^2}, \tag{A7}$$

where $\psi_i(t)$ is the wave function at the mech i at time t. When $\lambda(t)$ becomes exponentially large, the dynamical instability occurs. Fig. 11 (b) shows the time evolution of $\lambda(t)$ for the same parameter of Fig. 11 (a). The results show that the values of $\lambda(t)$ for branches (1) and (4) are less than 1 for all time while those for branches (2) and (3) are exponentially large after the instability occurs. From these results, we can conclude that branches (1) and (4) are stable and (2) and (3) are unstable. In the same manner, we can judge the stability for the exact solutions in other parameters.

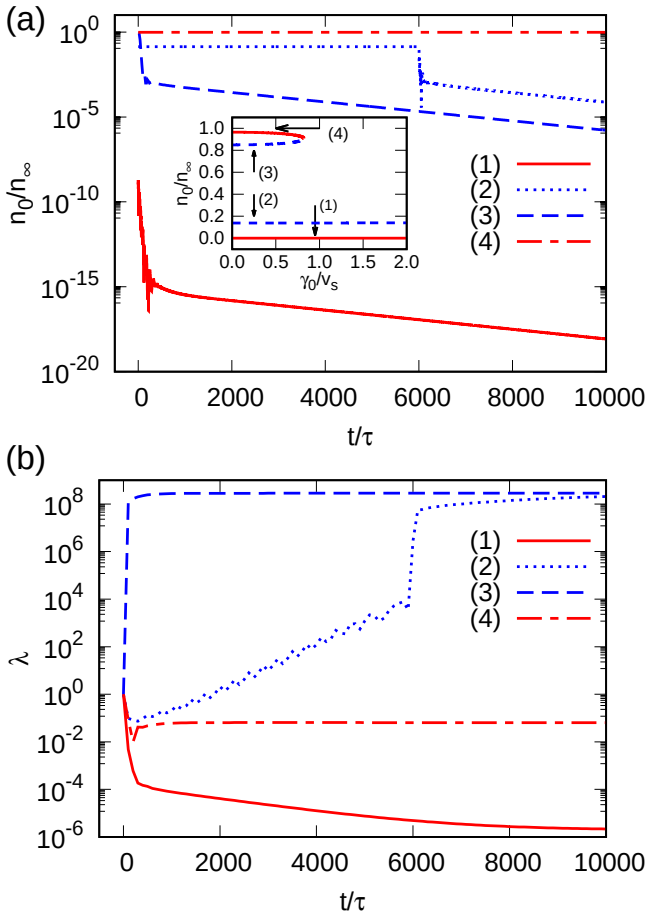

FIG. 11: (Color online) (a) Time evolution of n_0 of the type 3 for $U_0 = 1gn_\infty\xi$, $L = 2\xi$, and $\gamma_0 = 0.2v_{\rm s}$. The red (blue) curves represent the stable (unstable) states. The inset shows the correspondence of the results (1)-(4) to the n_0-γ_0 diagram of the type 3. (b) Time evolution of λ. The parameters are same as (a).

Appendix B: Details of the derivation of the exact solutions for the even function case

In this appendix, we describe the details of the derivation of the exact solutions for the even function case. As we described in Sec. III B, it is sufficient to consider only the region of $x > 0$.

First, we derive Eq. (25). From the boundary condition (4) and the equation of continuity (9), we obtain the current density in the stationary states as

$$J(x) = -{\rm sgn}(x)n_\infty v_\infty, \tag{B1}$$

where sgn$(\cdot)$ is the sign function. The boundary condition due to the local loss potential (8) can be written as

$$\left.\frac{dn(x)}{dx}\right|_{x=+0} = 0, \quad -\frac{\hbar^2}{M}\left.\frac{d\varphi(x)}{dx}\right|_{x=+0} = \frac{\hbar\gamma_0}{2}, \tag{B2}$$

where we used the assumption of the even function. Using the second equation of Eq. (B2) and the expression

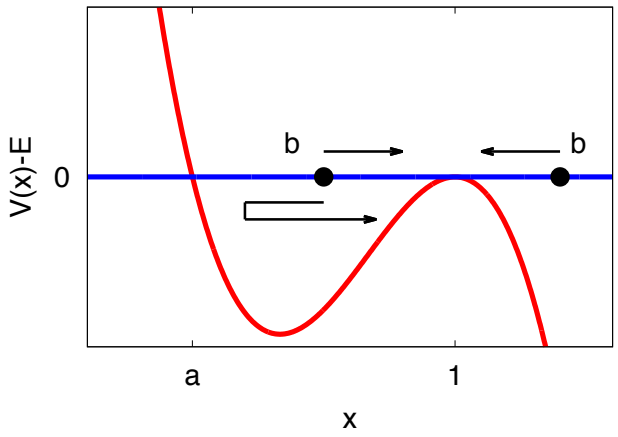

FIG. 12: (Color online) Schematic picture of the motion in the potential $V(x)$. The motion is possible in the region $V(x) - E \leq 0$. The arrows indicate the directions of the motion.

of the current density

$$J(x=+0) = \frac{\hbar}{M} n(0) \left.\frac{d\varphi(x)}{dx}\right|_{x=+0} = -n_\infty v_\infty, \quad \text{(B3)}$$

we obtain Eq. (25); $v_\infty = (n_0/n_\infty)\gamma_0/2$.

Then we consider to solve the GP equation. We define

$$C(x) \equiv \frac{\hbar^2}{2M}\left|\frac{d\Psi(x)}{dx}\right|^2 + \mu|\Psi(x)|^2 - \frac{g}{2}|\Psi(x)|^4. \quad \text{(B4)}$$

It can be easily shown that $C(x)$ is a constant for $0 \leq x \leq L$ and $x > L$. Substituting $\Psi(x) = \sqrt{n(x)}e^{i\varphi(x)}$ and $J(x)$ into Eq. (B4), we obtain

$$\frac{\hbar^2}{4Mg}\left[\frac{dn(x)}{dx}\right]^2 = n(x)^3 - \frac{2\mu}{g}n(x)^2 + \frac{2C(x)}{g}n(x) - \frac{M}{g}J(x)^2. \quad \text{(B5)}$$

Here, we consider the outside region ($x > L$). In this region, we obtain $C(x) = (1/2)gn_\infty^2 + Mv_\infty^2 n_\infty$ from the boundary condition at infinity (4). Equation (B5) in the outside region reduces to

$$\frac{\xi^2}{4}\left[\frac{dn_{\rm out}(x)/n_\infty}{dx}\right]^2 = \left[\frac{n_{\rm out}(x)}{n_\infty} - 1\right]^2\left[\frac{n_{\rm out}(x)}{n_\infty} - \left(\frac{v_\infty}{v_{\rm s}}\right)^2\right]. \quad \text{(B6)}$$

We mention that Eq. (B6) is related to the problem of the classical mechanics. Here, we consider a classical particle under the potential $V(x)$. In this case, the energy of the system is given by

$$\frac{1}{4}\left[\frac{dx(t)}{dt}\right]^2 + V(x(t)) = E$$
$$\Rightarrow \quad \frac{1}{4}\left[\frac{dx(t)}{dt}\right]^2 = E - V(x(t)), \quad \text{(B7)}$$

where $x(t)$ is a position of the classical particle at time t and we set the mass of the particle as $m = 1/2$ and E is the total energy. When $V(x) - E = -(x-1)^2(x-a)$ $(0 < a < 1)$, this equation is the same structure of Eq. (B6). We assume that $x(t \to \infty) = 1$, which corresponds to the boundary condition of the density $n_{\rm out}(x)/n_\infty \to 1$ at $x \to \infty$. From this, we can obtain the information of the motion under the potential $V(x)$ by an intuitive way. Figure 12 shows the potential. From Eq. (B7), the motion is possible only if $V(x) - E \leq 0$. Here, we set the initial condition $x(0) = b$. When $b \geq 1$, we obtain $dx(t)/dt \leq 0$. When $b < 1$, we have two cases: one is that $x(t)$ is monotonically approaching to 1 and the other is that $x(t)$ is bounced at $x(t) = a$ and goes to 1. The difference comes from the sign of the initial condition $dx(t)/dt|_{t=0}$.

From the above discussion, we can expect that there are three types of solutions in the outside region. From Eq. (B6) we obtain

$$\pm\frac{1}{2}\int_{n_L/n_\infty}^{n(x)/n_\infty} dX \frac{1}{|1-X|\sqrt{X - (v_\infty/v_{\rm s})^2}} = \frac{x-L}{\xi}. \quad \text{(B8)}$$

Here, we consider the case $n_L/n_\infty < 1$. In this case, we can show $n_L \leq n_{\rm out}(x) \leq n_\infty$ from Eq. (B6) and perform the integral in Eq. (B8), then we obtain Eq. (21):

$$\frac{n_{\rm out}(x)}{n_\infty} = \left(\frac{v_\infty}{v_{\rm s}}\right)^2 + \left[1 - \left(\frac{v_\infty}{v_{\rm s}}\right)^2\right] \times \tanh^2\left[\sqrt{1 - \left(\frac{v_\infty}{v_{\rm s}}\right)^2}\frac{x - L + x_+}{\xi}\right], \quad \text{(B9)}$$

$$\frac{x_+}{\xi} = \frac{1}{\sqrt{1 - \left(\frac{v_\infty}{v_{\rm s}}\right)^2}} \times \tanh^{-1}\left[\sqrt{\frac{n_L/n_\infty - (v_\infty/v_{\rm s})^2}{1 - (v_\infty/v_{\rm s})^2}}\right], \quad \text{(B10)}$$

To perform the integral, we used the following integral formula

$$\int dx \frac{1}{(px+q)\sqrt{ax+b}} = \frac{1}{\sqrt{(bp-aq)p}}\log\left|\frac{p\sqrt{ax+b} - \sqrt{(bp-aq)p}}{p\sqrt{ax+b} + \sqrt{(bp-aq)p}}\right|, \quad \text{(B11)}$$

where this formula is valid for $(bp - aq)p > 0$. In the case of $n_L/n_\infty > 1$, we can obtain the different solution, whose functional form is given by replacing tanh with coth in Eq. (21). However, we cannot find the parameter region where this solution satisfies the boundary conditions. Therefore, we do not consider the case $n_L/n_\infty > 1$ in the main part of the paper.

The phase of the outside region can be obtained by integrating Eq. (B3). Its expression is given by

$$\varphi_{\rm out}(x) = \varphi_L - \frac{Mv_\infty(x-L)}{\hbar} - \tan^{-1}\left[\frac{G(x+x_+)}{v_\infty/v_{\rm s}}\right] + \tan^{-1}\left[\frac{G(L+x_+)}{v_\infty/v_{\rm s}}\right], \tag{B12}$$

$$G(x) = \sqrt{1-\left(\frac{v_\infty}{v_{\rm s}}\right)^2}\tanh\left[\sqrt{1-\left(\frac{v_\infty}{v_{\rm s}}\right)^2}\frac{x-L}{\xi}\right], \tag{B13}$$

To perform the integral, we used the following mathematical formulae:

$$\frac{d}{dx}\tan^{-1}[F(x)] = \frac{\frac{dF(x)}{dx}}{1+[F(x)]^2}, \quad e^{i\tan^{-1}(x)} = \frac{1+ix}{\sqrt{1+x^2}}, \tag{B14}$$

where $F(x)$ is a smooth function.

We can obtain the constraint of the velocity v_∞ from the above results. From Eq. (B6), $n_{\rm out}(x)/n_\infty \geq (v_\infty/v_{\rm s})^2$ must hold. Using $n_{\rm out}(x)/n_\infty \leq 1$, we obtain the relation

$$\left(\frac{v_\infty}{v_{\rm s}}\right)^2 \leq 1 \quad \Rightarrow \quad \left(\frac{\gamma_0}{v_{\rm s}}\right)^2 \leq 4\left(\frac{n_\infty}{n_0}\right)^2. \tag{B15}$$

This means that the velocity of the stationary solution is always subsonic. This is consistent with the well known results for the condition of the existence of the gray soliton in uniform systems.

Now, we consider the inside region ($0 < x < L$). Using the first equation of Eq. (B2), Eqs. (25) and (B5), we can determine $C_{\rm in} \equiv C(x)$ (for $x < L$) in the inside region:

$$\frac{C_{\rm in}}{gn_\infty^2} = \frac{1}{8}\left(\frac{\gamma_0}{v_{\rm s}}\right)^2\frac{n_0}{n_\infty} + \left[1+\frac{1}{8}\left(\frac{\gamma_0}{v_{\rm s}}\right)^2\left(\frac{n_0}{n_\infty}\right)^2\right]\frac{n_0}{n_\infty} - \frac{1}{2}\left(\frac{n_0}{n_\infty}\right)^2. \tag{B16}$$

From Eq. (B16), we can rewrite (B5) in the inside region as

$$\frac{\xi^2}{4}\left[\frac{dn(x)/n_\infty}{dx}\right]^2 = \left[\frac{n(x)}{n_\infty}-\frac{n_0}{n_\infty}\right]\left[\frac{n(x)}{n_\infty}-A\right]\left[\frac{n(x)}{n_\infty}-B\right], \tag{B17}$$

where A and B were defined by Eqs. (32) and (33):

$$A = \frac{1}{2}\left[2+\frac{1}{4}\left(\frac{\gamma_0}{v_{\rm s}}\right)^2\left(\frac{n_0}{n_\infty}\right)^2 - \frac{n_0}{n_\infty} + \sqrt{\Delta}\right], \tag{B18}$$

$$B = \frac{1}{2}\left[2+\frac{1}{4}\left(\frac{\gamma_0}{v_{\rm s}}\right)^2\left(\frac{n_0}{n_\infty}\right)^2 - \frac{n_0}{n_\infty} - \sqrt{\Delta}\right], \tag{B19}$$

$$\Delta = \left[\frac{n_0}{n_\infty} - 2 - \frac{1}{4}\left(\frac{\gamma_0}{v_{\rm s}}\right)^2\left(\frac{n_0}{n_\infty}\right)^2\right]^2 - \left(\frac{\gamma_0}{v_{\rm s}}\right)^2\frac{n_0}{n_\infty}. \tag{B20}$$

We can integrate Eq. (B17) in a similar manner of the case of the outside region. The corresponding potential of the classical mechanics is given by

$$V(x) - E = -(x-x_0)(x-A)(x-B). \tag{B21}$$

In this case, the initial condition is given by $x(0) = x_0$, which corresponds to $n(x=0) = n_0$. To perform the integral, we need to know the relation between A and B. When $\Delta \geq 0$, we obtain $A \geq B$ from Eqs. (32), (33), and (34). Therefore, we classify the solutions as four types: Solution 1 : $\Delta \geq 0,\ B \leq x_0 \leq A$, Solution 2 : $\Delta \geq 0,\ x_0 \leq B \leq A$, Solution 3 : $\Delta \geq 0,\ B \leq A \leq x_0$, Solution 4 : $\Delta < 0$. The behavior of the potential is shown in Fig. 13.

Here, we consider the solution 1. From the inequalities $\Delta \geq 0$, $B \leq n_0/n_\infty \leq A$, and Eq. (B15), this solution exists in the region

$$\left(\frac{\gamma_0}{v_{\rm s}}\right)^2 \leq \frac{8}{1+n_0/n_\infty} \text{ and } 0 \leq \frac{n_0}{n_\infty} \leq 1. \tag{B22}$$

We plot the parameter region in Fig. 14. The solution1 [Eq. (26)] can be obtained by integration of Eq. (B17)

$$\frac{n_{\rm in}^{(1)}(x)}{n_\infty} = A - \left(A - \frac{n_0}{n_\infty}\right){\rm nd}^2(\Delta^{1/4}x/\xi|m_1), \tag{B23}$$

$$\varphi_{\rm in}^{(1)}(x) = -\frac{1}{2A}\frac{n_0}{n_\infty}\frac{\gamma_0}{v_{\rm s}}\frac{x}{\xi} - \frac{1}{2\Delta^{1/4}}\frac{\gamma_0}{v_{\rm s}}\frac{A-n_0/n_\infty}{A} \times \Pi[m_1 A/(n_0/n_\infty); {\rm am}(\Delta^{1/4}x/\xi|m_1)|m_1], \tag{B24}$$

$$m_1 = 1 - \frac{A-n_0/n_\infty}{\sqrt{\Delta}}, \tag{B25}$$

where we used the formula 17.4.63 in Ref. [63]. The phase (B24) is also obtained by integrating Eq. (B3). To perform this, integral, we used the following relations:

$$\Pi(n;\phi|m) = \int_0^\phi d\theta \frac{1}{(1-n\sin^2\theta)\sqrt{1-m\sin^2\theta}} = \int_0^{F(\phi|m)} dy \frac{1}{1-n{\rm sn}^2(y|m)}, \tag{B26}$$

$$\Pi[n;{\rm am}(x|m)|m] = \int_0^x dy \frac{1}{1-n{\rm sn}^2(y|m)}, \tag{B27}$$

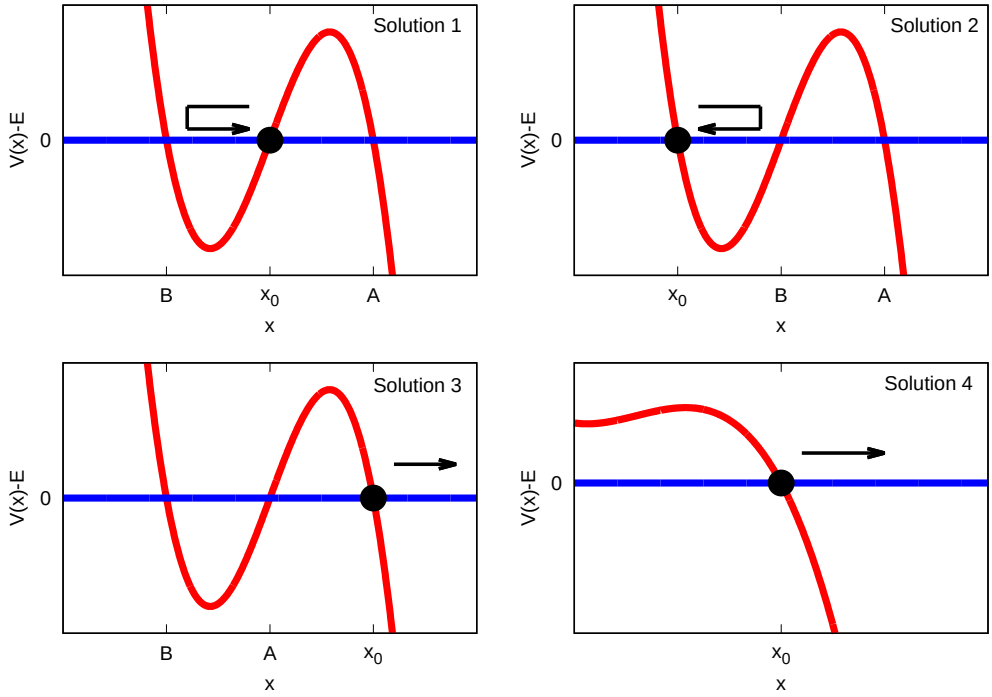

FIG. 13: (Color online) Schematic picture of the motion in the potential $V(x)$. The motion is possible in the region $V(x)-E \leq 0$. The arrows indicate the directions of the motion. In the solution 4, there is one solution $V(x) - E = 0$ hence A and $B = A^*$ are complex.

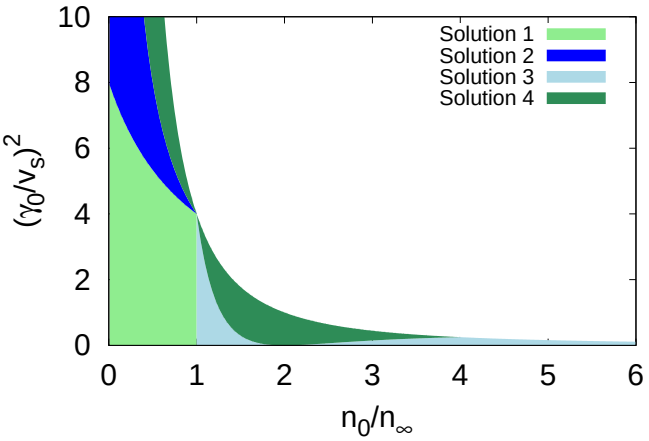

FIG. 14: (Color online) Parameter region for each solution.

where $F(\phi|m)$ is the incomplete elliptic integral of the first kind.

The region where the solution 2 exists is derived by $\Delta \geq 0$, $n_0/n_\infty \leq B \leq A$, and Eq. (B15):

$$\frac{8}{1+n_0/n_\infty} < \left(\frac{\gamma_0}{v_s}\right)^2 \leq \frac{4}{n_0/n_\infty} \text{ and } \frac{n_0}{n_\infty} \leq 1. \quad \text{(B28)}$$

The expression of the solution 2 is given by

$$\frac{n_{\rm in}^{(2)}(x)}{n_\infty} = \frac{n_0}{n_\infty} + \left(B - \frac{n_0}{n_\infty}\right) {\rm sn}^2(\Delta^{1/4}x/\xi|m_2), \quad \text{(B29)}$$

$$\varphi_{\rm in}^{(2)}(x) = -\frac{1}{2\Delta^{1/4}}\frac{\gamma_0}{v_s} \times \Pi\left[\frac{B-n_0/n_\infty}{n_0/n_\infty}; {\rm am}(\Delta^{1/4}x/\xi|m_2)\middle| m_2\right], \quad \text{(B30)}$$

$$m_2 = \frac{B-n_0/n_\infty}{A-n_0/n_\infty}. \quad \text{(B31)}$$

To obtain Eqs. (B29) and (B30), we used the formula 17.4.62 in Ref. [63].

The region of the solution 3 is derived by $\Delta \geq 0$, $B \leq A \leq n_0/n_\infty$, and Eq. (B15):

$$\left(\frac{\gamma_0}{v_s}\right)^2 \leq \frac{4(2-n_0/n_\infty)^2}{(n_0/n_\infty)^3} \text{ and } 1 < \frac{n_0}{n_\infty} \leq 4, \quad \text{(B32)}$$

$$\text{or } \left(\frac{\gamma_0}{v_s}\right)^2 \leq \frac{4}{(n_0/n_\infty)^2} \text{ and } 4 < \frac{n_0}{n_\infty}. \quad \text{(B33)}$$

The expression of the solution 3 is given by

$$\frac{n_{\rm in}^{(3)}(x)}{n_\infty} = \frac{n_0}{n_\infty} + \left(\frac{n_0}{n_\infty} - A\right) {\rm sc}^2\left(\frac{\Delta^{1/4}}{\sqrt{m_3}}\frac{x}{\xi}\middle| m_3\right), \tag{B34}$$

$$\begin{aligned}\varphi_{\rm in}^{(3)}(x) = &-\frac{\sqrt{m_3}}{2\Delta^{1/4}}\frac{n_0}{n_\infty}\frac{\gamma_0}{v_{\rm s}}\left\{\frac{\Delta^{1/4}x}{A\sqrt{m_3}\xi}\right.\\ &+\frac{A-n_0/n_\infty}{An_0/n_\infty}\\ &\left.\times\Pi\left[A/(n_0/n_\infty);{\rm am}(\Delta^{1/4}x/\sqrt{m_3}\xi|m_3)\middle| m_3\right]\right\},\end{aligned} \tag{B35}$$

$$m_3 \equiv \frac{\sqrt{\Delta}}{A_1+\sqrt{\Delta}}, \quad A_1 \equiv -\left(A - \frac{n_0}{n_\infty}\right), \tag{B36}$$

where ${\rm sc}(x|m) \equiv {\rm sn}(x|m)/{\rm cn}(x|m)$ and we used the formula 17.4.64 in Ref. [63].

The region of the solution 4 is derived by $\Delta < 0$ and Eq. (B15):

$$\frac{4}{n_0/n_\infty} < \left(\frac{\gamma_0}{v_{\rm s}}\right)^2 \le \frac{4}{(n_0/n_\infty)^2} \text{ and } \frac{n_0}{n_\infty} \le 1, \text{ or} \tag{B37}$$

$$\frac{4(2-n_0/n_\infty)^2}{(n_0/n_\infty)^3} < \left(\frac{\gamma_0}{v_{\rm s}}\right)^2 \le \frac{4}{(n_0/n_\infty)^2} \text{ and } 1 < \frac{n_0}{n_\infty} \le 4. \tag{B38}$$

The expression of the solution 4 is given by

$$\begin{aligned}\frac{n_{\rm in}^{(4)}(x)}{n_\infty} &= \frac{n_0}{n_\infty} + A_2\frac{1-{\rm cn}\left(2\sqrt{A_2}\frac{x}{\xi}\middle| m_4\right)}{1+{\rm cn}\left(2\sqrt{A_2}\frac{x}{\xi}\middle| m_4\right)}\\ &= \frac{n_0}{n_\infty} + A_2{\rm sc}^2(\sqrt{A_2}x/\xi|m_4){\rm dn}^2(\sqrt{A_2}x/\xi|m_4),\end{aligned} \tag{B39}$$

$$\begin{aligned}\varphi_{\rm in}^{(4)}(x) = &-\frac{1}{2\sqrt{A_2}}\frac{n_0}{n_\infty}\frac{\gamma_0}{v_{\rm s}}\frac{1}{m_4A_2(C_+-C_-)}\\ &\times\left\{(C_+^{-1}-1)\Pi\left[C_+^{-1};{\rm am}(\sqrt{A_2}x/\xi|m_4)\,|\,m_4\right]\right.\\ &\left.-(C_-^{-1}-1)\Pi\left[C_-^{-1};{\rm am}(\sqrt{A_2}x/\xi|m_4)\,|\,m_4\right]\right\},\end{aligned} \tag{B40}$$

where we defined

$$A_2 \equiv \sqrt{2\left(\frac{n_0}{n_\infty}\right)^2 - \left[2+\left(\frac{v_\infty}{v_{\rm s}}\right)^2\right]\frac{n_0}{n_\infty} + \left(\frac{v_\infty}{v_{\rm s}}\right)^2\frac{n_\infty}{n_0}}, \tag{B41}$$

$$m_4 \equiv \frac{1}{2A_2}\left[A_2 - \frac{3n_0}{2n_\infty} + 1 + \frac{1}{8}\left(\frac{\gamma_0}{v_{\rm s}}\right)^2\left(\frac{n_0}{n_\infty}\right)^2\right], \tag{B42}$$

$$C_\pm \equiv \frac{1}{2}\left(D \pm \sqrt{D^2 + \frac{4n_0/n_\infty}{m_4A_2}}\right), \tag{B43}$$

$$D \equiv \frac{A_2 - n_0/n_\infty}{m_4A_2}. \tag{B44}$$

Here, we used the formulae 16.18.4 and 17.4.71 in Ref. [63].

What remains to do is to determine the parameters n_L, φ_L, and n_0 by connecting the inside and the outside solutions via the boundary conditions. n_L and φ_L are determined by the first expression of Eq. (6), that is, $n_L^{(i)} = n_{\rm in}^{(i)}(x=L)$ and $\varphi_L^{(i)} = \varphi_{\rm in}^{(i)}(x=L)$. The explicit expressions for the density are given by

$$\frac{n_L^{(1)}}{n_\infty} = A - \left(A - \frac{n_0}{n_\infty}\right){\rm nd}^2(\Delta^{1/4}L/\xi|m_1), \tag{B45}$$

$$\frac{n_L^{(2)}}{n_\infty} = \frac{n_0}{n_\infty} + \left(B - \frac{n_0}{n_\infty}\right){\rm sn}^2(\Delta^{1/4}L/\xi|m_2), \tag{B46}$$

$$\frac{n_L^{(3)}}{n_\infty} = \frac{n_0}{n_\infty} + \left(\frac{n_0}{n_\infty} - A\right){\rm sc}^2\left(\frac{\Delta^{1/4}}{\sqrt{m_3}}\frac{L}{\xi}\middle| m_3\right), \tag{B47}$$

$$\frac{n_L^{(4)}}{n_\infty} = \frac{n_0}{n_\infty} + A_2{\rm sc}^2(\sqrt{A_2}L/\xi|m_4){\rm dn}^2(\sqrt{A_2}L/\xi|m_4). \tag{B48}$$

n_0 is determined by the boundary condition (8), which reduces to

$$\frac{\hbar^2}{4M}\left[\left.\frac{dn(x)}{dx}\right|_{x=L+0} - \left.\frac{dn(x)}{dx}\right|_{x=L-0}\right] = U_0n(L), \tag{B49}$$

$$\left.\frac{d\varphi(x)}{dx}\right|_{x=L+0} = \left.\frac{d\varphi(x)}{dx}\right|_{x=L-0}. \tag{B50}$$

Equation (B50) is automatically satisfied due to the expression of the current density (B3). Equation (B49)

reduces to

$$S_{\rm out}(i)\left|\frac{n_L^{(i)}}{n_\infty}-1\right|\sqrt{\frac{n_L^{(i)}}{n_\infty}-\frac{1}{4}\left(\frac{\gamma_0}{v_{\rm s}}\right)^2\left(\frac{n_0}{n_\infty}\right)^2}$$
$$-S_{\rm in}(i)\sqrt{\left[\frac{n_L^{(i)}}{n_\infty}-\frac{n_0}{n_\infty}\right]\left[\frac{n_L^{(i)}}{n_\infty}-A\right]\left[\frac{n_L^{(i)}}{n_\infty}-B\right]}$$
$$=\frac{2M\xi U_0}{\hbar^2}\frac{n_L^{(i)}}{n_\infty}, \tag{B51}$$

$$S_{\rm out}(i)\equiv{\rm sgn}\left[\left.\frac{dn_{\rm out}(x)}{dx}\right|_{x=L}\right]. \tag{B52}$$

$$S_{\rm in}(i)\equiv{\rm sgn}\left[\left.\frac{dn_{\rm in}^{(i)}(x)}{dx}\right|_{x=L}\right]. \tag{B53}$$

Because $n_L^{(i)}$ is a function of n_0, equation (B51) is a one-variable equation of n_0 for fixed γ_0 and U_0. Therefore, the problem to solve the GP equation (non-linear differential equation) reduces to solving the one-variable equation (B51). Because we cannot obtain the analytical solutions of Eq. (B51), we solve this equation numerically.

As we mentioned in the main part of the paper, we cannot find that the parameter region where the solution 3 and 4 satisfy the boundary conditions. This means that n_0/n_∞ moves only $0\le n_0/n_\infty\le 1$.

Appendix C: Details of the derivation of the exact solutions for the odd function case

In this appendix, we show the expression of the boundary condition (7) for the odd function case. Substituting Eqs. (36), (37), and (38) into Eq. (7), we obtain

$$\frac{e^{i\varphi_0}}{1+m_0}\left[1+m_0-2m_0{\rm sn}^2\left(\sqrt{\frac{2}{1+m_0}}\frac{L}{\xi}\middle|m_0\right)\right]$$
$$-\frac{2\sqrt{m_0}}{1+m_0}{\rm cn}\left(\sqrt{\frac{2}{1+m_0}}\frac{L}{\xi}\middle|m_0\right){\rm dn}\left(\sqrt{\frac{2}{1+m_0}}\frac{L}{\xi}\middle|m_0\right)$$
$$=\frac{2MU_0\xi}{\hbar^2}\sqrt{\frac{2m_0}{1+m_0}}{\rm sn}\left(\sqrt{\frac{2}{1+m_0}}\frac{L}{\xi}\middle|m_0\right), \tag{C1}$$

where φ_0 has been determined by Eq. (38).

[1] I. Bloch, J. Dalibard, and W. Zwerger, Rev. Mod. Phys. **80**, 885 (2008).
[2] A. Polkovnikov, K. Sengupta, A. Silva, and M. Vengalattore, Rev. Mod. Phys. **83**, 863 (2011).
[3] M. Rigol, V. Dunjko, and M. Olshanii, Nature **452**, 854 (2008).
[4] M. Gring, M. Kuhnert, T. Langen, T. Kitagawa, B. Rauer, M. Schreitl, I. Mazets, D. A. Smith, E. Demler, and J. Schmiedmayer, Science **337**, 1318 (2012)
[5] A. M. Kaufman, M. E. Tai, A. Lukin, M. Rispoli, R. Schittko, P. M. Preiss, and M. Greiner, Science **353**, 794 (2016).
[6] T. Mori, T. N. Ikeda, E. Kaminishi, and M. Ueda, J. Phys. B: At. Mol. Opt. Phys. **51**, 112001 (2018).
[7] M. Schreiber, S. S. Hodgman, P. Bordia, H. P. Lüschen, M. H. Fischer, R. Vosk, E. Altman, U. Schneider, and I. Bloch, Science **349**, 842 (2015).
[8] J. Smith, A. Lee, P. Richerme, B. Neyenhuis, P. W. Hess, P. Hauke, M. Heyl, D. A. Huse, and C. Monroe, Nat. Phys. **12**, 907 (2016).
[9] J.-y. Choi, S. Hild, J. Zeiher, P. Schauß, A. Rubio-Abadal, T. Yefsah, V. Khemani, D. A. Huse, I. Bloch, and C. Gross, Science **352**, 1547 (2016).
[10] R. Nandkishore and D. A. Huse, Annu. Rev. Condens. Matter Phys. **6**, 15 (2015).
[11] E. Altman and R. Vosk, Annu. Rev. Condens. Matter Phys. **6**, 383 (2015).
[12] D. A. Abanin, E. Altman, I. Bloch, and M. Serbyn, arXiv:1804.11065 (2018).
[13] N. Syassen, D. M. Bauer, M. Lettner, T. Volz, D. Dietze, J. J. Garcia-Ripoll, J. I. Cirac, G. Rempe, and S. Dürr, Science **320**, 1329 (2008).
[14] G. Barontini, R. Labouvie, F. Stubenrauch, A. Vogler, V. Guarrera, and H. Ott, Phys. Rev. Lett. **110**, 035302 (2013).
[15] B. Yan, S. A. Moses, B. Gadway, J. P. Covey, K. R. Hazzard, A. M. Rey, D. S. Jin, and J. Ye, Nature **501**, 521 (2013).
[16] R. Labouvie, B. Santra, S. Heun, S. Wimberger, and H. Ott, Phys. Rev. Lett. **115**, 050601 (2015).
[17] Y. S. Patil, S. Chakram, and M. Vengalattore, Phys. Rev. Lett. **115**, 140402 (2015).
[18] R. Labouvie, B. Santra, S. Heun, and H. Ott, Phys. Rev. Lett. **116**, 235302 (2016).
[19] H. P. Lüschen, P. Bordia, S. S. Hodgman, M. Schreiber, S. Sarkar, A. J. Daley, M. H. Fischer, E. Altman, I. Bloch, and U. Schneider, Phys. Rev. X **7**, 011034 (2017).
[20] T. Tomita, S. Nakajima, I. Danshita, Y. Takasu, and Y. Takahashi, Sci. Adv. **3**, e1701513 (2017).
[21] S. Diehl, A. Micheli, A. Kantian, B. Kraus, H. P. Büchler, and P. Zoller, Nat. Phys. **4**, 878 (2008).
[22] F. Verstraete, M. M. Wolf, and J. I. Cirac, Nat. Phys. **5**, 633 (2009).
[23] A. J. Daley, Adv. Phys. **63**, 77 (2014).
[24] Y. Ashida, S. Furukawa, and M. Ueda, Phys. Rev. A **94**, 053615 (2016).
[25] B. Misra and E. C. G. Sudarshan, J. Math. Phys. **18**, 756 (1977).
[26] M. J. Mark, E. Haller, K. Lauber, J. G. Danzl, A. Janisch, H. P. Büchler, A. J. Daley, and H.-C. Nägerl, Phys. Rev. Lett. **108**, 215302 (2012).
[27] C. M. Bender and S. Boettcher, Phys. Rev. Lett. **80**, 5243 (1998).
[28] C. E. Rüter, K. G. Makris, R. El-Ganainy, D. N. Christodoulides, M. Segev, and D. Kip, Nat. Phys. **6**, 192 (2010).
[29] V. V. Konotop, J. Yang, and D. A. Zezyulin, Rev. Mod. Phys. **88**, 035002 (2016),

[30] L. Xiao, X. Zhan, Z. H. Bian, K. K. Wang, X. Zhang, X. P. Wang, J. Li, K. Mochizuki, D. Kim, N. Kawakami, W. Yi, H. Obuse, B. C. Sanders, and P. Xue, Nat. Phys. **13**, 1117 (2017).

[31] J. Li, A. K. Harter, J. Liu, L. de Melo, Y. N. Joglekar, and L. Luo, Nat. Comm. **10**, 855 (2019).

[32] C. M. Bender, Rep. Prog. Phys. **70**, 947 (2008).

[33] R. El-Ganainy, K. G. Makris, M. Khajavikhan, Z. H. Musslimani, S. Rotter, and D. N. Christodoulides, Nat. Phys. **14**, 11 (2018).

[34] Z. Gong, Y. Ashida, K. Kawabata, K. Takasan, S. Higashikawa, and M. Ueda, Phys. Rev. X **8**, 031079 (2018).

[35] M. Kunimi and I. Danshita, Phys. Rev. A **99**, 043613 (2019).

[36] V. A. Brazhnyi, V. V. Konotop, V. M. Pérez-García, and H. Ott, Phys. Rev. Lett. **102**, 144101 (2009).

[37] D. Sels and E. Demler, arXiv:1809.10516.

[38] D. Yamamoto, I. Danshita, and C. A. R. Sá de Melo, Phys. Rev. A **85**, 021601(R) (2012).

[39] D. Yamamoto and I. Danshita, Phys. Rev. B **88**, 014419 (2013).

[40] D. Yamamoto, T. Ozaki, C. A. R. Sá de Melo, and I. Danshita, Phys. Rev. A **88**, 033624 (2013).

[41] In the infinite systems, the naive definition of the total particle number $N_{\rm naive}(t) \equiv \int_{-\infty}^{+\infty} dx n(x,t)$ is ill defined because it diverges under the boundary condition (4). Therefore, we must consider the total particle number difference as in the main text.

[42] L. D. Landau, J. Phys. (USSR) **5**, 71 (1941).

[43] B. Wu and Q. Niu, New J. Phys. **5**, 104 (2003).

[44] A. Baratoff, J. A. Blackburn, and B. B. Schwartz, Phys. Rev. Lett. **25**, 1096 (1970).

[45] F. Sols and J. Ferrer, Phys. Rev. B **49**, 15913 (1994).

[46] V. Hakim, Phys. Rev. E **55**, 2835 (1997).

[47] D. L. Kovrizhin, Phys. Lett. A **287**, 392 (2001).

[48] C. T. Pham and M. Brachet, Physica D **163**, 127 (2002).

[49] N. Pavloff, Phys. Rev. A **66**, 013610 (2002).

[50] Y. Kagan, D. L. Kovrizhin, and L. A. Maksimov, Phys. Rev. Lett. **90**, 130402 (2003).

[51] G. E. Astrakharchik and L. P. Pitaevskii, Phys. Rev. A **70**, 013608 (2004).

[52] B. T. Seaman, L. D. Carr, and M. J. Holland, Phys. Rev. A **71**, 033609 (2005).

[53] N. Bilas and N. Pavloff, Phys. Rev. A **72**, 033618 (2005).

[54] I. Danshita, N. Yokoshi, and S. Kurihara, New J. Phys. **8**, 44 (2006).

[55] I. Danshita and S. Tsuchiya, Phys. Rev. A **75**, 033612 (2007).

[56] G. Watanabe, F. Dalfovo, F. Piazza, L. P. Pitaevskii, and S. Stringari, Phys. Rev. A **80**, 053602 (2009).

[57] A. G. Sykes, M. J. Davis, and D. C. Roberts, Phys. Rev. Lett. **103**, 085302 (2009).

[58] D. Takahashi and Y. Kato, J. Phys. Soc. Jpn. **78**, 023001 (2009).

[59] F. Piazza, L. A. Collins, and A. Smerzi, Phys. Rev. A **81**, 033613 (2010).

[60] Y. Kato and S. Watabe, Phys. Rev. Lett. **105**, 035302 (2010).

[61] S. Watabe and Y. Kato, Phys. Rev. A **88**, 063612 (2013).

[62] M. Cominotti, D. Rossini, M. Rizzi, F. Hekking, and A. Minguzzi, Phys. Rev. Lett. **113**, 025301 (2014).

[63] M. Abramowitz and I. A. Stegun, *Handbook of Mathematical Functions* (National Bureau of Standards, Washington, DC, 1964).

[64] S. H. Strogatz, *Nonlinear Dynamics and Chaos: With Applications to Physics, Biology, Chemistry, and Engineering* (Addison-Wesley, Reading, MA, 1994).

[65] S. Nakamura, Phys. Rev. Lett. **109**, 120602 (2012).

[66] M. T. Reeves, T. P. Billam, B. P. Anderson, and A. S. Bradley, Phys. Rev. Lett. **114**, 155302 (2015).

[67] A. C. Cassidy, D. Mason, V. Dunjko, and M. Olshanii, Phys. Rev. Lett. **102**, 025302 (2009).